Acta Cryst. (1975). A31, 345

Growth Spirals and Complex Polytypism in Micas. I. Polytypic Structure Generation

BY ALAIN BARONNET

Laboratoire de Minéralogie–Cristallographie, Laboratoire des Mécanismes de la Croissance Cristalline, Université d'Aix-Marseille III, *Centre Scientifique Saint Jérome*, 13397 *Marseille Cédex* 4, *France*

(*Received* 11 *October* 1974; *accepted* 16 *January* 1975)

The possible polytypic structures of a mica monocrystal are generated, using a single screw dislocation emerging on both (001) faces. The discussion takes into account: (1) each basic structure the crystallite may have during its previous layer-by-layer growth, (2) the number and position of the elementary layers of the crystal when the spiral becomes active, (3) the Burgers vector strength of the dislocation. Deduced new polytypic structures, belonging to different structural series, are described and their positions with respect to the different basic structures are discussed. Some well-known growth features in micas such as 'epitaxic overgrowths' and 'macroscopic' twinning may, in some cases, be connected with a spiral growth mechanism. The layer-stacking sequences of complex polytypic structures of natural and synthetic micas reported thus far in the literature can be compared with the predictions of the screw dislocation theory of polytypism on perfect or more or less faulted basic structures.

I. Introduction

Several different theories as reported by Verma & Krishna (1966), have been put forth by various workers to account for the phenomenon of polytypism in crystals. Attempts to unify them have been so far unsuccessful. However, polytypism as a result of growth spiral activity connected with the occurrence of screw dislocations (Frank, 1949, 1951) in crystals seems to be the theory which receives the most evident experimental confirmations on various polytypic compounds such as SiC, CdI_2 and ZnS. Nevertheless, the screw dislocation theory alone does not give an exhaustive answer to this problem. If the theory fairly satisfactorily explains the generation of long-period polytypes, it does not account for the occurrence of common basic structures on which the former structures are frequently based. Keeping this in view, Mitchell (1957) and Krishna & Verma (1965) derived the theoretically possible polytypes of SiC assuming screw dislocations of various strengths created on the different basic structures of this compound. This work resulted in the derivation of structural series in which most of the X-ray determined polytypes could be classified.

Mica polytypism and polymorphism were first attributed by Amelinckx & Dekeyser (1953) to a spiral growth mechanism operating on a disordered layer-grown structure. Subsequent numerous detailed X-ray structural studies (Hendricks & Jefferson, 1939; Rieder, 1970; Ross, Takeda & Wones, 1966; Smith & Yoder, 1966; Takeda, 1967*a*, 1969, 1971; Takeda & Mackay, 1969) have shown the high observation frequency of a limited number of short-period polymorphs in this mineral family. Moreover, layer-stacking sequence analyses of long-period polytypes (L.P.P.) reveal that they are often based on the short-period polymorphs. More recently (Baronnet, 1972*a*, *b*, 1973; Baronnet, Amouric & Chabot, 1975) studies on synthetic phlogopite and muscovite using surface microtopographic methods of electron microscopy demonstrated the dominant roles played by the nucleation and/or layer-by-layer growth processes during the building of polymorphs and by spiral growth in the generation of complex polytypes. In the case of spiral growth, it was experimentally shown that a layer-grown structure occurs before the screw dislocation originates in the crystallite. The succession of these two mechanisms during the growth of a single crystal leads us to deduce the theoretically possible polytypic structures in micas similar to those of Krishna & Verma (1965) for SiC.

In the present paper, the 'ideal' structure of the mica structural unit is briefly given in order to introduce polytypism/polymorphism notations and representation. Then, the most likely basic structures of micas are reviewed. The structural issues of the occurrence of growth spirals on each basic structure are examined and the deduced polytypic structures are then compared with the complex polytypes already reported in the literature.

II. Deduced and observed polytypic structures

II.1 *Mica single-layer structure and polytypism/polymorphism notations*

The actual structure of the mica single layer depends mainly upon its chemical composition and to a lesser extent upon the polymorph concerned. Nevertheless, for the sake of simplicity, only the 'ideal' structure described by Pauling (1930) and Jackson & West (1931, 1933) will be reported here. The single layer is composed of two sixfold tetrahedral sheets sandwiching a single octahedral sheet ($\frac{2}{1}$ phyllosilicate layer type). The structure of the latter sheet is mainly governed by close packing of O atoms located at the vertices of

both tetrahedral sheets. Adjacent single layers are linked together by interlayer cations. These interlayer cations occupy vacancies created by the tetrahedral rings bounding the interlayer region. The mica 'ideal' structural unit is monoclinic, space group $C2/m$ (Pabst, 1955). Lattice parameter relationships are as follows: $b=3^{1/2}a$, $\beta=\cos^{-1}(-a/3c)$. Therefore, the C-centred plane unit cell (Fig. 1) is shifted by a layer stagger (or stacking vector) $\mathbf{t}_n=-\frac{1}{3}\mathbf{a}_n$ from a unit layer n to the next one $n+1$. $\mathbf{t}_{n+1}$ may adopt six different orientations with respect to $\mathbf{t}_n$ so that the interlayer stacking angle (Smith & Yoder, 1956) will be $(\mathbf{t}_n,\mathbf{t}_{n+1})=0 \bmod \pi/3$. In the ideal structure approximation, each of these adjoining layer configurations keeps the interlayer cation coordination polyhedra unchanged. Mica polytypism is described by the stacking mode of N adjacent layers; this stacking sequence repeats after every Nth layer. The R.T.W. polytype designation of Ross *et al.* (1966) is adopted throughout this paper. The R.T.W. symbols are based first on Ramsdell's (1947) notation where the number of layers is followed by the symmetry symbol of the unit cell (*Tc*, *M*, *O*, *T* and *H* for triclinic, monoclinic, orthorhombic, trigonal and hexagonal respectively). Stacking symbols $0, \pm 1, \pm 2$ or 3 which refer respectively to $0°, \pm 60°, \pm 120°, 180°$ interlayer stacking angles are given within brackets [Fig. 2(*b*)]. As the R.T.W. notation is orientation-free, Zvyagin's layer position symbols (Zvyagin, 1962) are adjoined [Fig. 2(*a*)] to the above notation and put in parentheses. The C-layer standard position is chosen as opposite to the 5·3 Å lattice vector of the involved basic structure or polymorph.

II.2 *Basic structures of micas*

$1M[0](C)$, $1Mr\,n(120)$,* $2M_2[1\bar{1}](A\bar{B})$, $3T[222](ABC)$ and $2M_1[2\bar{2}](\bar{A}\bar{B})$ are the most commonly found structures of micas. The first three are considered to be the most 'stable' stacking modes of trioctahedral micas whereas the two last forms are more frequently encountered among dioctahedral species. $1M[0](C)$ (Baronnet, 1972*a*, *b*; Ross *et al.*, 1966), $2M_1[2\bar{2}](\bar{A}\bar{B})$ (Baronnet *et al.*, 1975; Takeda, 1969), $3T[222](ABC)$ (Ross *et al.*, 1966; Takeda, 1967*a*) and $1Mr\,n(120)$ (Baronnet, 1972*a*, *b*) were also identified as substructures of complex polytypes. $1Mr\,n(60)$,† theoretically considered by Ross *et al.* (1966), may be regarded as a possible basic structure of F-bearing trioctahedral micas [*e.g.* the $4Tc[0231](\bar{C}\bar{C}\bar{A}A)$ (Takeda, 1967*b*) complex polytype of synthetic lithium–fluorophlogopite appears to be based on such a stacking mode, see § II.4] To our knowledge, L.P.P. based on $2M_2[1\bar{1}](A\bar{B})$ have not yet been reported. Nevertheless, as this structure occurs frequently among some natural Li-bearing micas (Foster, 1960; Munoz, 1968), it is regarded as a possible basic structure below. Note that $3T[\bar{2}\bar{2}\bar{2}](ACB)$, the enantiomorphic stacking sequence of $3T[222](ABC)$, may be also considered as a basic structure since the former was recently found as well as the latter in synthetic OH-muscovite (Baronnet *et al.*, 1975). Among $2O[33](C\bar{C})$, $6H[111111](C\bar{B}A\bar{C}B\bar{A})$ and $6H[\bar{1}\bar{1}\bar{1}\bar{1}\bar{1}\bar{1}](C\bar{A}B\bar{C}A\bar{B})$ structures theoretically derived by Smith & Yoder (1956), only the first was recently found (Giuseppetti & Tadini, 1972) to be an actual stacking scheme in the brittle mica anandite and therefore is retained below. All the six periodic basic structures are considered as stacking-fault-free in the following deductive section.

II.3 *Generation of the polytypic structures induced by spiral growth*

Let us consider a plate-like perfect crystallite previously grown according to the layer-by-layer growth mechanism. Subsequently, a single dislocation of mainly screw character is created, the dislocation line of which crosses the platelet. Accordingly, two different exposed ledges appear, one on each of the well developed (001) and (00$\bar{1}$) faces of the flattened mica crystal. The equal numbers of layers N_s exposed on both faces are determined by the modulus $N_s\times 10$ Å of the Burgers-vector component normal to {001}. Hence, two spirals are assumed to be active on the same crystal, subsequently leading to the growth of two

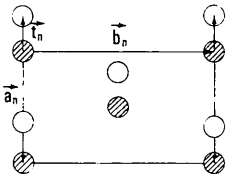

Fig. 1. The C-centred monoclinic cell of the mica single layer. Striped circles: lower interlayer cations. Open circles: upper interlayer cations. $\mathbf{t}_n$ is the normal projection onto (001) of the c single layer parameter. The graphical representation of polytypes and polymorphs of Smith & Yoder (1956) is a chain of arrows corresponding to the succession of the $\mathbf{t}_n$ vectors through the crystal.

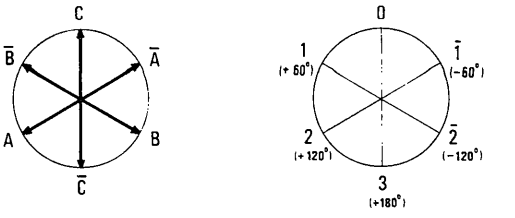

(*a*) (*b*)

Fig. 2. (*a*) Single-layer position symbols of Zvyagin (1963). Each symbol refers to the $\mathbf{t}_n$ orientation. The standard layer orientation C is chosen as opposite to the 5·3 Å lattice vector of the basic structure. (*b*) Interlayer stacking angle symbols of Ross *et al.* (1966). They refer to stacking angles between adjacent single layers.

* $1Mr\,n(120)$ refers to aperiodic structures, the successive interlayer stacking angles of which are $n\times 120°$. The successive values of n are randomly (r) chosen among 0,1 and 2.

† $1Mr\,n(60)$ describes aperiodic structures, the successive interlayer stacking angles of which are $n\times 60°$. The successive values of n are randomly (r) chosen among 0, 1, 2, 3, 4 and 5.

polytypic structures sandwiching the initial structure of the platelet, *i.e.* the basic structure. The initial platelet, at the instant when the dislocation arises, is composed of N_c layers. There is no reason to think that N_c would correspond to a whole number of N, with N being the periodicity of the basic structure. As stated above, N_s layers are exposed on both {001} faces: these layers are respectively numbered $1,2,3\ldots,N_s-1$, N_s on $(00\bar{1})$ and N_c-N_s+1, $N_c-N_s+2,\ldots,N_c-1$, N_c on (001). The stacking vector $\mathbf{t}_n$ is assumed to remain pointing in the same direction within any one layer n as the spiral winds itself around the dislocation core. Note that the dislocation sign by no means affects the polytypic structure to be generated. Consider A_n and a_n respectively as Zvyagin's position symbol of the layer n and the R.T.W. stacking-angle symbol between adjacent layers n and $n+1$. Then, the platelet basic structure may be represented by the double series:

$$\begin{matrix}(A_1 & A_2 & A_3\ldots A_{N_c-2} & A_{N_c-1} & A_{N_c})\\ a_1 & a_2 & a_3\ldots & a_{N_c-2} & a_{N_c-1}\,.\end{matrix}$$

Left and right series terms refer respectively to surface structures near $(00\bar{1})$ and (001) faces. At the moment when the dislocation involving N_s exposed layers originates, the structure on both sides of the slip plane is:

$$\begin{matrix}a_1 & a_2 & a_3\ldots a_{N_s} & a_{N_s+1}\ldots\\ \underbrace{A_1 & A_2 & A_3\ldots A_{N_s}}_{\text{Lower exposed ledge}} & A_{N_s+1}\ldots\\ & & A_1 & A_2\ldots\\ & & a_1 & a_2\ldots\end{matrix}$$

$$\begin{matrix}\ldots a_{N_c-1} & \text{Upper exposed ledge}\\ \ldots A_{N_c-1} & A_{N_c}\\ \ldots A_{N_c-N_s} & A_{N_c-N_s+1}\ldots A_{N_c-1} & A_{N_c}\\ \ldots a_{N_c-N_s} & \ldots\ldots\ldots a_{N_c-1}\end{matrix}$$

where superposed Zvyagin's symbols indicate that the corresponding layers are situated at the same level on both sides of the slip plane. The respective lower and upper spirals create the following respective stacking sequences during winding downwards and upwards:

$$\begin{matrix}(a_1 & a_2\ldots a_{N_s-1} & a_0)_p & a_1 & a_2\ldots a_{N_s-1} & a_{N_s}\ldots\\ \underbrace{(A_1 & A_2 & A_3\ldots A_{N_s})_p}_{\text{Lower spiral}} & \underbrace{|A_1 & A_2 & A_3\ldots A_{N_s}|\ldots}_{\text{Lower exposed ledge}}\end{matrix}$$

$$\begin{matrix}a_{N_c-N_s} & a_{N_c-N_s+1}\ldots\ldots\ldots\ldots a_{N_c-1}\\ \underbrace{|A_{N_c-N_s+1} & A_{N_c-N_s+2}\ldots A_{N_c-1} & A_{N_c}|}_{\text{Upper exposed ledge}}\end{matrix}$$

$$\begin{matrix}(a_{00} & a_{N_c-N_s+1} & a_{N_c-N_s+2}\ldots\ldots a_{N_c-1})_q\\ \underbrace{(A_{N_c-N_s+1} & A_{N_c-N_s+2}\ldots\ldots A_{N_c-1} & A_{N_c})_q}_{\text{Upper spiral}}\end{matrix}$$

with p and q the number of turns of each growth spiral. If, on one hand, in the induced polytypic structures, all Zvyagin's symbols are inherited from a part of the basic structure, on the other, two new R.T.W. symbols a_0 and a_{00} appear at the bottom of the exposed ledges. a_0 and a_{00} replace a_{N_s} and $a_{N_c-N_s}$ respectively. They are generated by stacking of the layer 1 under layer N_s and of layer N_c-N_s+1 upon N_c. Knowing the basic structure stacking sequence, N_s and N_c values and the position of the last layer N_c, a_0 and a_{00} are easily inferred from the periodicity conditions (Ross *et al.*, 1966; Takeda, 1971) keeping R.T.W. symbols:

$$a_0+\sum_{n=1}^{n=N_s-1}a_n=0 \bmod 6 \text{ and } a_{00}+\sum_{n=N_c-N_s+1}^{n=N_c-1}a_n=0 \bmod 6.$$

By following Takeda (1971) we will treat the R.T.W. symbol series of a given stacking sequence as a series of numbers. Two algebraic properties of these series are of interest to understand the forthcoming deductions: (1) a cyclic permutation of the numbers means only that the origin of the sequence is shifted and therefore does not change the stacking sequence itself; (2) taking the supplement of the series describes an enantiomorph of the initial structure.

$N_s \leq N_c$ must be obeyed for a layer to be present at the bottom of each exposed ledge.

Finally, the structure of the dislocated crystal as a whole may be written as follows:

$$\begin{matrix}(a_1 & a_2 & a_3\ldots a_{N_s-1} & a_0)_p & a_1 & a_2\ldots\\ (A_1 & A_2 & A_3\ldots\ldots A_{N_s})_p & A_1 & A_2 & A_3\ldots\end{matrix}$$

$$\begin{matrix}\ldots a_{N_c-1} & (a_{00} & a_{N_c-N_s+1} & a_{N_c-N_s+2}\ldots a_{N_c-1})_q\\ \ldots A_{N_c} & (A_{N_c-N_s+1} & A_{N_c-N_s+2}\ldots\ldots A_{N_c})_q\,.\end{matrix}$$

The above symbol series will be expressed now considering the possible mica basic structures and then taking into account: (1) the layer number N_s in the exposed ledges, (2) the layer number N_c of the perfect platelet just before the dislocation appears, (3) the orientation of the layer N_c. Note that the orientation of layer 1 is connected with the orientation of N_c in the case of periodic basic structures, if the N_c value is known.

II.3.1 *Growth spirals on the basic* $1M[0](C)$ *structure*

$1M[0](C)$ may be developed as: $\ldots C\ C\ C\ C\ C\ldots$
$\ldots\ 0\ 0\ 0\ 0\ldots$

It is obvious that whatever values N_c and N_s may adopt, the spirals will reproduce respectively p and q times the layer stacking sequence $[0]_{N_s}(C)_{N_s}$, *i.e.* $1M[0](C)$. In other words, whatever the strength of the screw dislocation, the $1M[0](C)$ grows further by the spiral growth mechanism (see Fig. 3) without introduction of any stacking fault.

II.3.2 *Growth spirals on the basic* $2M_1[2\bar{2}](\bar{A}\bar{B})$ *structure*

The periodic $2M_1[2\bar{2}](\bar{A}\bar{B})$ stacking sequence is written below:

$\ldots\bar{A}\ \bar{B}\ \bar{A}\ \bar{B}\ \bar{A}\ \bar{B}\ldots$
$\ldots\ 2\ \bar{2}\ 2\ \bar{2}\ 2\ \bar{2}\ldots$

Four possibilities (i, ii, iii, iv) exist for the end surface structures of the initial crystal platelet, depending upon N_c value and last-layer position:

$N_c = 2 \bmod 2$* (i) $A_{N_c} = \vec{A}$: $\bar{B}\,\vec{A}\,\bar{B}\,\vec{A}\ldots\bar{B}\,\vec{A}\,\bar{B}\,\vec{A}$ / $\bar{2}\;2\;\bar{2}\;\ldots\;\bar{2}\;2\;\bar{2}$

(ii) $A_{N_c} = \bar{B}$: $\vec{A}\,\bar{B}\,\vec{A}\,\bar{B}\ldots\vec{A}\,\bar{B}\,\vec{A}\,\bar{B}$ / $2\;\bar{2}\;2\;\ldots\;2\;\bar{2}\;2$

$N_c = 1 \bmod 2$ (iii) $A_{N_c} = \vec{A}$: $\vec{A}\,\bar{B}\,\vec{A}\,\bar{B}\ldots\bar{B}\,\vec{A}\,\bar{B}\,\vec{A}$ / $2\;\bar{2}\;2\;\ldots\;\bar{2}\;2\;\bar{2}$

(iv) $A_{N_c} = \bar{B}$: $\bar{B}\,\vec{A}\,\bar{B}\,\vec{A}\ldots\vec{A}\,\bar{B}\,\vec{A}\,\bar{B}$ / $\bar{2}\;2\;\bar{2}\;\ldots\;2\;\bar{2}\;2$

All the structures of a crystal including various N_s-layered spirals on it are listed in Table 1. For $N_s = 2 \bmod 2$, the structure $2M_1[2\bar{2}](\vec{A}\bar{B})$ grows further without occurrence of any stacking fault since $[\bar{2}2]_{(N_s/2)} = [2\bar{2}]_{(N_s/2)} = 2M_1[2\bar{2}]$. As $N_s = 3 \bmod 2$, two enantiomorphic† polytypic series are generated;

$$N_s Tc[(2\bar{2})_{(N_s-1)/2}0]\{(\vec{A}\bar{B})_{(N_s-1)/2}\vec{A}\}$$

and

$$N_s Tc[(\bar{2}2)_{(N_s-1)/2}0]\{(\bar{B}\vec{A})_{(N_s-1)/2}\bar{B}\}\,.$$

The two polytypic structures sandwiching the basic structure in the same crystal may be either the same ones in parallel positioning (iii and iv), or enantiomorphs (i and ii); see Fig. 4. For $N_s = 1$, the two spiral-grown $1M[0]$ structures are either parallel (iii and iv)

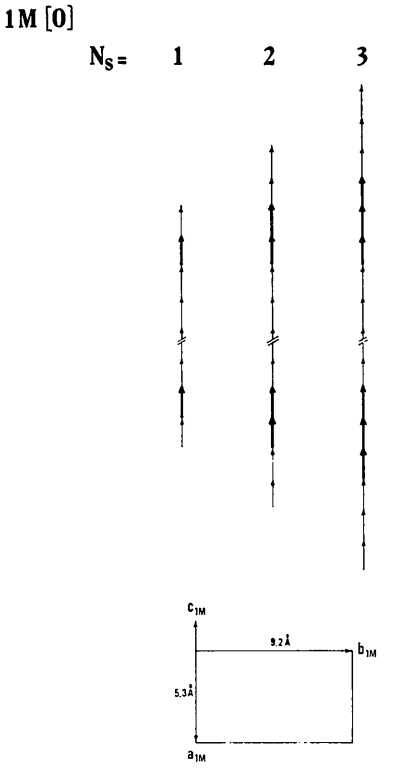

Fig. 3. Crystal polytypic structure representations using diagrams of Smith & Yoder. Spirals on $1M[0]$, $N_s = 1$, 2, and 3. To follow the arrow series means to describe the structure from bottom to top. Heavy arrows refer to the structure of the exposed ledges. Crystal structure drawings correspond to a unique turn of spirals ($p = q = 1$) on (001) and (00$\bar{1}$). In some cases, a second turn is drawn: dashed outer arrows in the diagrams.

* $i \bmod j$ means $i + kj$ with k as a positive integer when used to characterize N_s and N_c.

† From a pure structural point of view, these two series correspond to the same structure since they are deducible from each other by a twofold axis lying in the (001) plane. Nevertheless, as they may produce two distinct spiral growth patterns on a given growth face (Baronnet *et al.*, 1975), they are distinguished here. The same remark holds for later-reported structures generated by $N_s = 3 \bmod 2$ spirals on the $2M_2[1\bar{1}]$ basic structure.

Table 1. *Structures resulting from dislocations of $2M_1$ basic structure*

Dislocation strength	Perfect platelet structure		Crystal structure		
N_s	N_c	A_{N_c}	Lower part	Middle part	Upper part
1	2 mod 2	$\vec{A}$	$1M[0]\,(\bar{B})$	$2M_1[2\bar{2}]\,(\vec{A}\bar{B})$ (i)	$1M[0]\,(\vec{A})$
	2 mod 2	$\bar{B}$	$1M[0]\,(\vec{A})$	$2M_1[2\bar{2}]\,(\vec{A}\bar{B})$ (ii)	$1M[0]\,(\bar{B})$
	1 mod 2	$\vec{A}$	$1M[0]\,(\vec{A})$	$2M_1[2\bar{2}]\,(\vec{A}\bar{B})$ (iii)	$1M[0]\,(\vec{A})$
	1 mod 2	$\bar{B}$	$1M[0]\,(\bar{B})$	$2M_1[2\bar{2}]\,(\vec{A}\bar{B})$ (iv)	$1M[0]\,(\bar{B})$
2	2 mod 2	$\vec{A}$	$2M_1[\bar{2}2]\,(\bar{B}\vec{A})$	$2M_1[2\bar{2}]\,(\vec{A}\bar{B})$ (i)	$2M_1[2\bar{2}]\,(\bar{B}\vec{A})$
	2 mod 2	$\bar{B}$	$2M_1[2\bar{2}]\,(\vec{A}\bar{B})$	$2M_1[2\bar{2}]\,(\vec{A}\bar{B})$ (ii)	$2M_1[\bar{2}2]\,(\vec{A}\bar{B})$
	3 mod 2	$\vec{A}$	$2M_1[2\bar{2}]\,(\vec{A}\bar{B})$	$2M_1[2\bar{2}]\,(\vec{A}\bar{B})$ (iii)	$2M_1[2\bar{2}]\,(\bar{B}\vec{A})$
	3 mod 2	$\bar{B}$	$2M_1[\bar{2}2]\,(\bar{B}\vec{A})$	$2M_1[2\bar{2}]\,(\vec{A}\bar{B})$ (iv)	$2M_1[\bar{2}2]\,(\vec{A}\bar{B})$
3	4 mod 2	$\vec{A}$	$3Tc[\bar{2}20]\,(\bar{B}\vec{A}\bar{B})$	$2M_1[2\bar{2}]\,(\vec{A}\bar{B})$ (i)	$3Tc[02\bar{2}]\,(\vec{A}\bar{B}\vec{A})$
	4 mod 2	$\bar{B}$	$3Tc[2\bar{2}0]\,(\vec{A}\bar{B}\vec{A})$	$2M_1[2\bar{2}]\,(\vec{A}\bar{B})$ (iii)	$3Tc[0\bar{2}2]\,(\bar{B}\vec{A}\bar{B})$
	3 mod 2	$\vec{A}$	$3Tc[2\bar{2}0]\,(\vec{A}\bar{B}\vec{A})$	$2M_1[2\bar{2}]\,(\vec{A}\bar{B})$ (ii)	$3Tc[0\bar{2}2]\,(\vec{A}\bar{B}\vec{A})$
	3 mod 2	$\bar{B}$	$3Tc[\bar{2}20]\,(\bar{B}\vec{A}\bar{B})$	$2M_1[2\bar{2}]\,(\vec{A}\bar{B})$ (iv)	$3Tc[0\bar{2}2]\,(\bar{B}\vec{A}\bar{B})$
4	4 mod 2	$\vec{A}$	$2M_1[22]_2\,(\bar{B}\vec{A})_2$	$2M_1[2\bar{2}]\,(\vec{A}\bar{B})$ (i)	$2M_1[2\bar{2}]_2\,(\bar{B}\vec{A})_2$
	4 mod 2	$\bar{B}$	$2M_1[2\bar{2}]_2\,(\vec{A}\bar{B})_2$	$2M_1[2\bar{2}]\,(\vec{A}\bar{B})$ (ii)	$2M_1[\bar{2}2]\,(\vec{A}\bar{B})_2$
	5 mod 2	$\vec{A}$	$2M_1[2\bar{2}]_2\,(\vec{A}\bar{B})_2$	$2M_1[2\bar{2}]\,(\vec{A}\bar{B})$ (iii)	$2M_1[\bar{2}2]_2\,(\bar{B}\vec{A})_2$
	5 mod 2	$\bar{B}$	$2M_1[\bar{2}2]_2\,(\bar{B}\vec{A})_2$	$2M_1[2\bar{2}]\,(\vec{A}\bar{B})$ (iv)	$2M_1[\bar{2}2]_2\,(\vec{A}\bar{B})_2$
5	6 mod 2	$\vec{A}$	$5Tc[(\bar{2}2)_20]\,\{(\bar{B}\vec{A})_2\bar{B}\}$	$2M_1[2\bar{2}]\,(\vec{A}\bar{B})$ (i)	$5Tc[0(2\bar{2})_2]\,\{\vec{A}(\bar{B}\vec{A})_2\}$
	6 mod 2	$\bar{B}$	$5Tc[(2\bar{2})_20]\,\{(\vec{A}\bar{B})_2\vec{A}\}$	$2M_1[2\bar{2}]\,(\vec{A}\bar{B})$ (ii)	$5Tc[0(\bar{2}2)_2]\,\{\bar{B}(\vec{A}\bar{B})_2\}$
	5 mod 2	$\vec{A}$	$5Tc[(2\bar{2})_20]\,\{(\vec{A}\bar{B})_2\vec{A}\}$	$2M_1[2\bar{2}]\,(\vec{A}\bar{B})$ (iii)	$5Tc[0(2\bar{2})_2]\,\{\vec{A}(\bar{B}\vec{A})_2\}$
	5 mod 2	$\bar{B}$	$5Tc[(\bar{2}2)_20]\,\{(\bar{B}\vec{A})_2\bar{B}\}$	$2M_1[2\bar{2}]\,(\vec{A}\bar{B})$ (iv)	$5Tc[0(\bar{2}2)_2]\,\{\bar{B}(\vec{A}\bar{B})_2\}$

or in twinned position (i and ii). Note that the two entire crystal structures corresponding to $N_s=1$ mod 2 and $N_c=1$ mod 2 [Fig. 4 (iii) and (iv)] may be deduced from each other through a [010] twofold operation.

II.3.3 *Growth spirals on the basic* $2M_2[1\bar{1}](A\bar{B})$ *structure*

$2M_2[1\bar{1}](A\bar{B})$ basic structure is expressed as:

$$\begin{array}{l}\ldots A\ \bar{B}\ A\ \bar{B}\ A\ \bar{B}\ A\ \bar{B}\ldots\\ \ldots\ \bar{1}\ 1\ \bar{1}\ 1\ \bar{1}\ 1\ \bar{1}\ \ldots\end{array}$$

The different platelet structures are easily obtained from the $2M_1$ cases if we substitute A for $\bar{A}$, 1 for $\bar{2}$ and $\bar{1}$ for 2. It follows:

$N_c=2$ mod 2 (i) $A_{N_c}=A$: $\bar{B}\ A\ \bar{B}\ A\ \bar{B}\ldots\bar{B}\ A\ \bar{B}\ A$
$1\ \bar{1}\ 1\ \bar{1}\ \ldots\ 1\ \bar{1}\ 1$

(ii) $A_{N_c}=\bar{B}$: $A\ \bar{B}\ A\ \bar{B}\ldots A\ \bar{B}\ A\ \bar{B}$
$\bar{1}\ 1\ \bar{1}\ \ldots\ \bar{1}\ 1\ \bar{1}$

$N_c=1$ mod 2 (iii) $A_{N_c}=A$: $A\ \bar{B}\ A\ \bar{B}\ldots\bar{B}\ A\ \bar{B}\ A$
$\bar{1}\ 1\ \bar{1}\ \ldots\ 1\ \bar{1}\ 1$

(iv) $A_{N_c}=\bar{B}$: $\bar{B}\ A\ \bar{B}\ A\ldots A\ \bar{B}\ A\ \bar{B}$
$1\ \bar{1}\ 1\ \ldots\ \bar{1}\ 1\ \bar{1}$.

Table 2 lists all theoretical dislocated crystal structures up to $N_s=5$. For $N_s=2$ mod 2, the initial basic structure grows further on both sides of the crystal, stacking-fault-free. For $N_s=3$ mod 2, the two enantiomorphic $N_sTc[(1\bar{1})_{(N_s-1)/2}0]\{(\bar{B}A)_{(N_s-1)/2}\bar{B}\}$ and $N_sTc[(\bar{1}1)_{(N_s-1)/2}0]\{(A\bar{B})_{(N_s-1)/2}A\}$ polytypic structure series are generated. The crystal outer structures are either of the same nature and parallel-positioned (iii and iv) or enantiomorphic (i and ii): see Fig. 4. For $N_s=1$, $1M[0]$ structures are either parallel (iii and iv) or in twinned position (i and ii). Note that the two entire crystal structures corresponding to $N_s=1$ mod 2 and $N_c=1$ mod 2 [Fig. 4. (iii) and (iv)] may be derived from each other by a $[010]_{2M_2}$ twofold operation.

II.3.4 *Growth spirals on the basic* $2O[33](C\bar{C})$ *structure*

At first examination, four perfect-crystal configurations in the $2O$ basic structure:

$$\begin{array}{l}\ldots C\ \bar{C}\ C\ \bar{C}\ C\ \bar{C}\ldots\\ \ldots.\ 3\ 3\ 3\ 3\ 3\ldots.\end{array}$$

need be considered, that is:

$N_c=2$ mod 2 (i) $A_{N_c}=C$: $\bar{C}\ C\ \bar{C}\ldots C\ \bar{C}\ C$
$3\ 3\ \ldots\ 3\ 3$

$A_{N_c}=\bar{C}$: $C\ \bar{C}\ C\ldots\bar{C}\ C\ \bar{C}$
$3\ 3\ \ldots\ 3\ 3$

$N_c=1$ mod 2 (ii) $A_{N_c}=C$: $C\ \bar{C}\ C\ldots C\ \bar{C}\ C$
$3\ 3\ \ldots\ 3\ 3$

$A_{N_c}=\bar{C}$: $\bar{C}\ C\ \bar{C}\ldots\bar{C}\ C\ \bar{C}$
$3\ 3\ \ldots\ 3\ 3$.

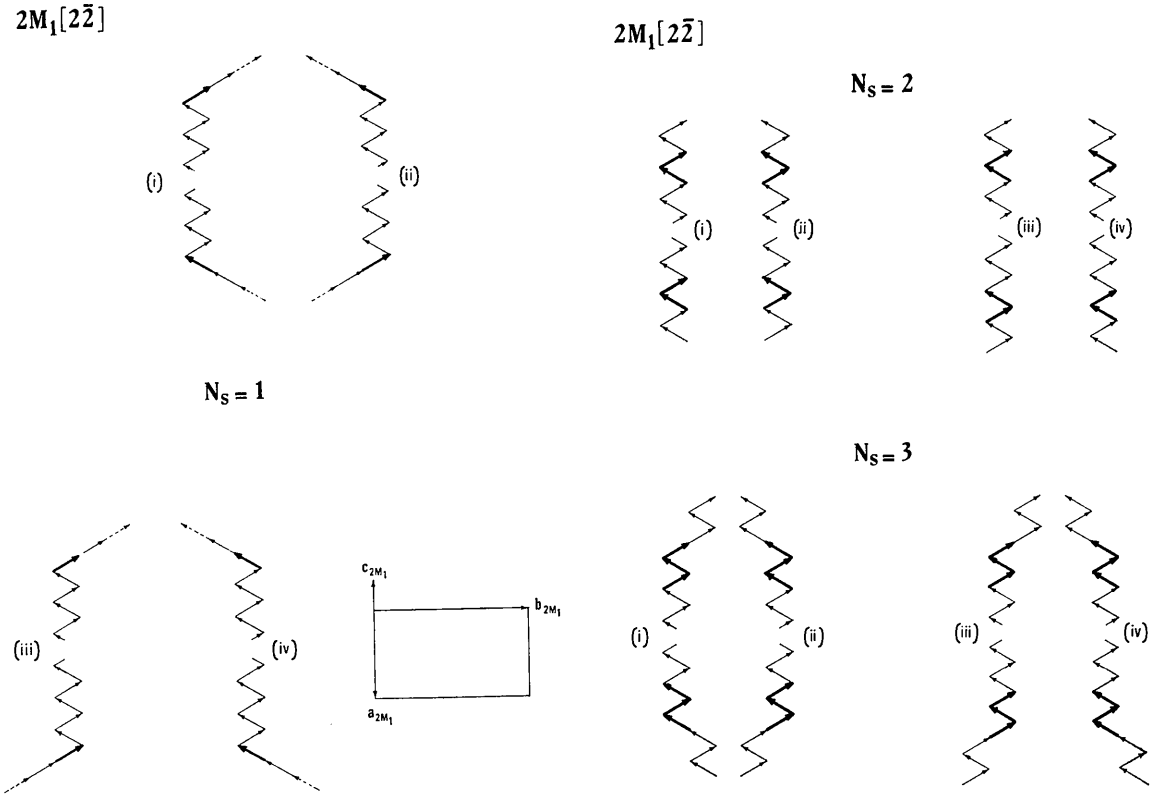

Fig. 4. Spirals on the two-layer basic structures: $2M_1[2\bar{2}]$, $2M_2[1\bar{1}]$ and $2O[33]$, $N_s=1$, 2 and 3. Regarding the $2O$ case, superposed arrows are disjoined. From left to right, the structure is described from bottom to top. For full explanation of symbols, see caption to Fig. 3.

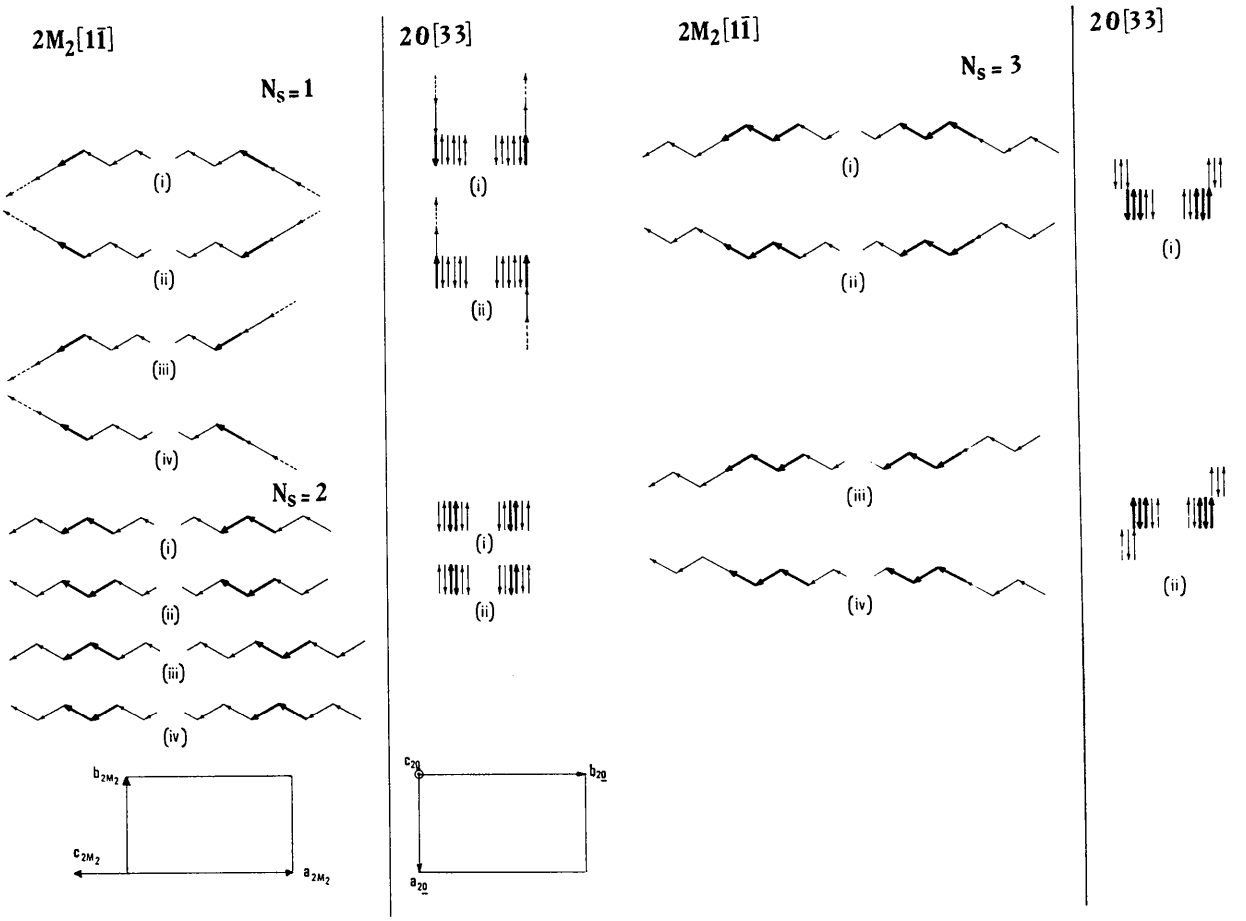

Fig. 4 (*cont.*)

Table 2. *Structures resulting from dislocations of* $2M_2$ *basic structure*

Dislocation strength	Perfect platelet structure		Crystal structure		
N_s	N_c	A_{N_c}	Lower part	Middle part	Upper part
1	2 mod 2	A	$1M[0]$ $(\bar{B})$	$2M_2[1\bar{1}]$ $(A\bar{B})$ (i)	$1M[0]$ (A)
	2 mod 2	$\bar{B}$	$1M[0]$ (A)	$2M_2[1\bar{1}]$ $(A\bar{B})$ (ii)	$1M[0]$ $(\bar{B})$
	1 mod 2	A	$1M[0]$ (A)	$2M_2[1\bar{1}]$ $(A\bar{B})$ (iii)	$1M[0]$ (A)
	1 mod 2	$\bar{B}$	$1M[0]$ $(\bar{B})$	$2M_2[1\bar{1}]$ $(A\bar{B})$ (iv)	$1M[0]$ $(\bar{B})$
2	2 mod 2	A	$2M_2[1\bar{1}]$ $(\bar{B}A)$	$2M_2[1\bar{1}]$ $(A\bar{B})$ (i)	$2M_2[\bar{1}1]$ $(\bar{B}A)$
	2 mod 2	$\bar{B}$	$2M_2[\bar{1}1]$ $(A\bar{B})$	$2M_2[1\bar{1}]$ $(A\bar{B})$ (ii)	$2M_2[1\bar{1}]$ $(A\bar{B})$
	3 mod 2	A	$2M_2[\bar{1}1]$ $(A\bar{B})$	$2M_2[1\bar{1}]$ $(A\bar{B})$ (iii)	$2M_2[\bar{1}1]$ $(\bar{B}A)$
	3 mod 2	$\bar{B}$	$2M_2[1\bar{1}]$ $(\bar{B}A)$	$2M_2[1\bar{1}]$ $(A\bar{B})$ (iv)	$2M_2[1\bar{1}]$ $(A\bar{B})$
3	4 mod 2	A	$3Tc[1\bar{1}0]$ $(\bar{B}A\bar{B})$	$2M_2[1\bar{1}]$ $(A\bar{B})$ (i)	$3Tc[0\bar{1}1]$ $(A\bar{B}A)$
	4 mod 2	$\bar{B}$	$3Tc[\bar{1}10]$ $(A\bar{B}A)$	$2M_2[1\bar{1}]$ $(A\bar{B})$ (ii)	$3Tc[01\bar{1}]$ $(\bar{B}A\bar{B})$
	3 mod 2	A	$3Tc[\bar{1}10]$ $(A\bar{B}A)$	$2M_2[1\bar{1}]$ $(A\bar{B})$ (iii)	$3Tc[0\bar{1}1]$ $(A\bar{B}A)$
	3 mod 2	$\bar{B}$	$3Tc[1\bar{1}0]$ $(\bar{B}A\bar{B})$	$2M_2[1\bar{1}]$ $(A\bar{B})$ (iv)	$3Tc[01\bar{1}]$ $(\bar{B}A\bar{B})$
4	4 mod 2	A	$2M_2[1\bar{1}]_2$ $(\bar{B}A)_2$	$2M_2[1\bar{1}]$ $(A\bar{B})$ (i)	$2M_2[\bar{1}1]_2$ $(\bar{B}A)_2$
	4 mod 2	$\bar{B}$	$2M_2[\bar{1}1]_2$ $(A\bar{B})_2$	$2M_2[1\bar{1}]$ $(A\bar{B})$ (ii)	$2M_2[1\bar{1}]_2$ $(A\bar{B})_2$
	5 mod 2	A	$2M_2[\bar{1}1]_2$ $(A\bar{B})_2$	$2M_2[1\bar{1}]$ $(A\bar{B})$ (iii)	$2M_2[\bar{1}1]_2$ $(\bar{B}A)_2$
	5 mod 2	$\bar{B}$	$2M_2[1\bar{1}]_2$ $(\bar{B}A)_2$	$2M_2[1\bar{1}]$ $(A\bar{B})$ (iv)	$2M_2[1\bar{1}]_2(A\bar{B})_2$
5	6 mod 2	A	$5Tc[(1\bar{1})_20]$ $\{(\bar{B}A)_2\bar{B}\}$	$2M_2[1\bar{1}]$ $(A\bar{B})$ (i)	$5Tc[0(\bar{1}1)_2]$ $\{A(\bar{B}A)_2\}$
	6 mod 2	$\bar{B}$	$5Tc[(\bar{1}1)_20]$ $\{(A\bar{B})_2A\}$	$2M_2[1\bar{1}]$ $(A\bar{B})$ (ii)	$5Tc[0(1\bar{1})_2]$ $\{\bar{B}(A\bar{B})_2\}$
	5 mod 2	A	$5Tc[(\bar{1}1)_20]$ $\{(A\bar{B})_2A\}$	$2M_2[1\bar{1}]$ $(A\bar{B})$ (iii)	$5Tc[0(\bar{1}1)_2]$ $\{A(\bar{B}A)_2\}$
	5 mod 2	$\bar{B}$	$5Tc[(1\bar{1})_20]$ $\{(\bar{B}A)_2\bar{B}\}$	$2M_2[1\bar{1}]$ $(A\bar{B})$ (iv)	$5Tc[0(1\bar{1})_2]$ $\{\bar{B}(A\bar{B})_2\}$

These four cases may be reduced to two (i and ii), taking into account that for each N_c value the two structures corresponding to $A_{N_c}=\bar{C}$ and $A_{N_c}=C$ are equivalent, except for a rotation through 180° about [001] of the $2O$ cell. The complete structures of crystals on which two spirals of $N_s \times 10$ Å pitch are active are given in Table 3. For $N_s=2$ mod 2, $2O[33]$ grows further on (001) and (00$\bar{1}$) faces. For $N_s=3$ mod 2, terms of a single structural series, $N_sM[(33]_{(N_s-1)/2}0]$-$\{(C\bar{C})_{(N_s-1)/2}C\}$ are derived and are simultaneously on both sides of the basic structure either in parallel – (i) or in twin positioning – (ii). See Fig. 4.

II.3.5 *Growth spirals on the basic* $3T[222](ABC)$ *structure*

The $3T$ structure may be written as follows:

$$\begin{array}{l} \ldots A\ B\ C\ A\ B\ C\ A\ B\ C\ldots \\ \ldots .2\ 2\ 2\ 2\ 2\ 2\ 2\ 2\ldots . \end{array}$$

Nine different platelet structure possibilities are distinguished below:

A_{N_c}	N_c	3 mod 3
C		$ABCA\ldots$(i)$\ldots CABC$
A		$BCAB\ldots\ldots\ldots ABCA$
B		$CABC\ldots\ldots\ldots BCAB$

1 mod 3	2 mod 3
$CABC\ldots$(ii)$\ldots CABC$	$BCAB\ldots$(iii)$\ldots CABC$
$ABCA\ldots\ldots\ldots ABCA$	$CABC\ldots\ldots\ldots ABCA$
$BCAB\ldots\ldots\ldots BCAB$	$ABCA\ldots\ldots\ldots BCAB$.

As the successive configurations in each column are derived from each other by a circular permutation operating on Zvyagin's symbols, these structures are equivalent, except for a rotation through 0 mod $2\pi/3$ about [0001] in the $3T$ cell. These cases may, therefore, be reduced to three (i, ii and iii). Table 4 lists all structure possibilities up to $N_s=5$. $N_s=3$ mod 3 results in the further growth of the $3T$ basic structure whereas $N_s=1$ mod 3 leads to $N_sM[(222)_{(N_s-1)/3}0]$-$\{(CAB)_{(N_s-1)/3}C\}$ and $N_s=2$ mod 3 to $N_sM[(22\bar{2})_{(N_s-2)/3}2\bar{2}]\{(ABC)_{(N_s-2)/3}AB\}$ polytype series. In Fig. 5 it is easily seen that the same spiral-grown polytype occurs on both basal faces of a given crystal and also that they are either parallel or connected by a twin operation.

II.3.6 *Growth spirals on the basic* $3T[\overline{222}](ACB)$ *structure*

The $3T[\overline{222}](ACB)$ layer-stacking sequence is developed as:

Table 3. *Structures resulting from dislocations of* $2O$ *basic structure*

Dislocation strength	Perfect platelet structure		Crystal structure		
N_s	N_c	A_{N_c}	Lower part	Middle part	Upper part
1	2 mod 2	C	$1M[0]\ (\bar{C})$	$2O[33]\ (C\bar{C})$ (i)	$1M[0]\ (C)$
	1 mod 2	C	$1M[0]\ (C)$	$2O[33]\ (C\bar{C})$ (ii)	$1M[0]\ (C)$
2	2 mod 2	C	$2O[33]\ (\bar{C}C)$	$2O[33]\ (C\bar{C})$ (i)	$2O[33]\ (\bar{C}C)$
	3 mod 2	C	$2O[33]\ (C\bar{C})$	$2O[33]\ (C\bar{C})$ (ii)	$2O[33]\ (\bar{C}C)$
3	4 mod 2	C	$3M[330]\ (\bar{C}C\bar{C})$	$2O[33]\ (C\bar{C})$ (i)	$3M[033]\ (C\bar{C}C)$
	3 mod 2	C	$3M[330]\ (C\bar{C}C)$	$2O[33]\ (C\bar{C})$ (ii)	$3M[033]\ (C\bar{C}C)$
4	4 mod 2	C	$2O[33]_2\ (\bar{C}C)_2$	$2O[33]\ (C\bar{C})$ (i)	$2O[33]_2\ (\bar{C}C)_2$
	5 mod 2	C	$2O[33]_2\ (C\bar{C})_2$	$2O[33]\ (C\bar{C})$ (ii)	$2O[33]_2\ (\bar{C}C)_2$
5	6 mod 2	C	$5M[(33)_20]\ \{(\bar{C}C)_2\bar{C}\}$	$2O[33]\ (C\bar{C})$ (i)	$5M[0(33)_2]\ \{(C\bar{C})_2C\}$
	5 mod 2	C	$5M[(33)_20]\ \{(C\bar{C})_2C\}$	$2O[33]\ (C\bar{C})$ (ii)	$5M[0(33)_2]\ \{(C\bar{C})_2C\}$

Table 4. *Structures resulting from dislocations of* $3T$ *basic structure*

Dislocation strength	Perfect platelet structure		Crystal structure		
N_s	N_c	A_{N_c}	Lower part	Middle part	Upper part
1	3 mod 3	C	$1M[0]\ (A)$	$3T[222]\ (ABC)$ (i)	$1M[0]\ (C)$
	1 mod 3	C	$1M[0]\ (C)$	$3T[222]\ (ABC)$ (ii)	$1M[0]\ (C)$
	2 mod 3	C	$1M[0]\ (B)$	$3T[222]\ (ABC)$ (iii)	$1M[0]\ (C)$
2	3 mod 3	C	$2M_1[2\bar{2}]\ (AB)$	$3T[222]\ (ABC)$ (i)	$2M_1[\bar{2}2]\ (BC)$
	4 mod 3	C	$2M_1[2\bar{2}]\ (CA)$	$3T[222]\ (ABC)$ (ii)	$2M_1[\bar{2}2]\ (BC)$
	2 mod 3	C	$2M_1[2\bar{2}]\ (BC)$	$3T[222]\ (ABC)$ (iii)	$2M_1[\bar{2}2]\ (BC)$
3	3 mod 3	C	$3T[222]\ (ABC)$	$3T[222]\ (ABC)$ (i)	$3T[222]\ (ABC)$
	4 mod 3	C	$3T[222]\ (CAB)$	$3T[222]\ (ABC)$ (ii)	$3T[222]\ (ABC)$
	5 mod 3	C	$3T[222]\ (BCA)$	$3T[222]\ (ABC)$ (iii)	$3T[222]\ (ABC)$
4	6 mod 3	C	$4M[2220]\ (ABCA)$	$3T[222]\ (ABC)$ (i)	$4M[0222]\ (CABC)$
	4 mod 3	C	$4M[2220]\ (CABC)$	$3T[222]\ (ABC)$ (ii)	$4M[0222]\ (CABC)$
	5 mod 3	C	$4M[2220]\ (BCAB)$	$3T[222]\ (ABC)$ (iii)	$4M[0222]\ (CABC)$
5	6 mod 3	C	$5M[(222)2\bar{2}]\ (ABCAB)$	$3T[222]\ (ABC)$ (i)	$5M[\bar{2}2(222)]\ (BCABC)$
	7 mod 3	C	$5M[(222)2\bar{2}]\ (CABCA)$	$3T[222]\ (ABC)$ (ii)	$5M[\bar{2}2(222)]\ (BCABC)$
	5 mod 3	C	$5M[(222)2\bar{2}]\ (BCABC)$	$3T[222]\ (ABC)$ (iii)	$5M[\bar{2}2(222)]\ (BCABC)$

$$\begin{array}{l} \ldots A\ C\ B\ A\ C\ B\ A\ C\ B \ldots \\ \ldots\ \bar{2}\ \bar{2}\ \bar{2}\ \bar{2}\ \bar{2}\ \bar{2}\ \bar{2}\ \bar{2}\ \ldots \end{array}$$

The three irreducible different platelet configurations are considered below, *i.e.*:

$N_c = 3 \bmod 3$ (i) $B\ A\ C\ B\ A\ C \ldots B\ A\ C\ B\ A\ C$
$= 1 \bmod 3$ (ii) $C\ B\ A\ C\ B\ A \ldots B\ A\ C\ B\ A\ C$
$= 2 \bmod 3$ (iii) $A\ C\ B\ A\ C\ B \ldots B\ A\ C\ B\ A\ C$.

A deductive approach similar to that reported above for the $3T[222](ABC)$ basic structure leads to whole-crystal structures that are respectively the enantiomorphs of those derived on the aforesaid basic structure. Hence, the two $N_sM[(\bar{2}\bar{2}\bar{2})_{(N_s-1)/3}0]$-$\{(BAC)_{(N_s-1)/3}B\}$ and $N_sM[(\bar{2}\bar{2}\bar{2})_{(N_s-2)/3}2\bar{2}]$-$\{(CBA)_{(N_s-2)/3}CB\}$ polytypic series result respectively from $N_s = 1 \bmod 3$ and $N_s = 2 \bmod 3$. The basic structure $3T[\bar{2}\bar{2}\bar{2}]$ grows further when $N_s = 3 \bmod 3$.

II.3.7 *Growth spirals on the disordered* $1Mr\ n(120)$ *and* $1Mr\ n(60)$ *basic structures*

As far as aperiodic basic structures are concerned, the number of expectable layer-stacking sequences within an exposed ledge becomes rapidly very large as N_s increases. Furthermore, the two spiral-grown polytypes on both {001} faces are no longer correlated in their structures except in their identical periodicities. Table 5 and 6 list the expectable polytypes grown by Frank's mechanism respectively on $1Mr\ n(120)$ when N_s ranges from 1 to 4 and on $1Mr\ n(60)$ when N_s ranges from 1 to 3.

Table 5. *Polytypic structures that may be generated by spirals on the basic* $1Mr\ n(120)$ *structure*

N_s	
1	$1M[0]$
2	$1M[0]$, $2M_1[2\bar{2}]$
3	$1M[0]$, $3Tc[02\bar{2}]$, $3Tc'[0\bar{2}2]$
	$3T[222]$, $3T[\bar{2}\bar{2}\bar{2}]$
4	$1M[0]$, $2M_1[2\bar{2}]$, $4M[020\bar{2}]$
	$4M[2220]$, $4M'[\bar{2}\bar{2}20]$, $4M[2\bar{2}\bar{2}2]$
	$4Tc[002\bar{2}]$, $4Tc'[00\bar{2}2]$

Table 6. *Polytypic structures that may be generated by spirals on the basic* $1Mr\ n(60)$ *structure*

N_s	
1	$1M[0]$
2	$1M[0]$, $2M_1[2\bar{2}]$, $2M_2[1\bar{1}]$, $2O[33]$
3	$1M[0]$, $3Tc[02\bar{2}]$, $3Tc'[0\bar{2}2]$, $3Tc[01\bar{1}]$, $3Tc'[0\bar{1}1]$
	$3M[033]$, $3M[11\bar{2}]$, $3M'[\bar{1}\bar{1}2]$, $3Tc[123]$, $3Tc'[\bar{1}23]$
	$3T[222]$, $3T'[\bar{2}\bar{2}\bar{2}]$, $3Tc[321]$, $3Tc'[\bar{3}2\bar{1}]$

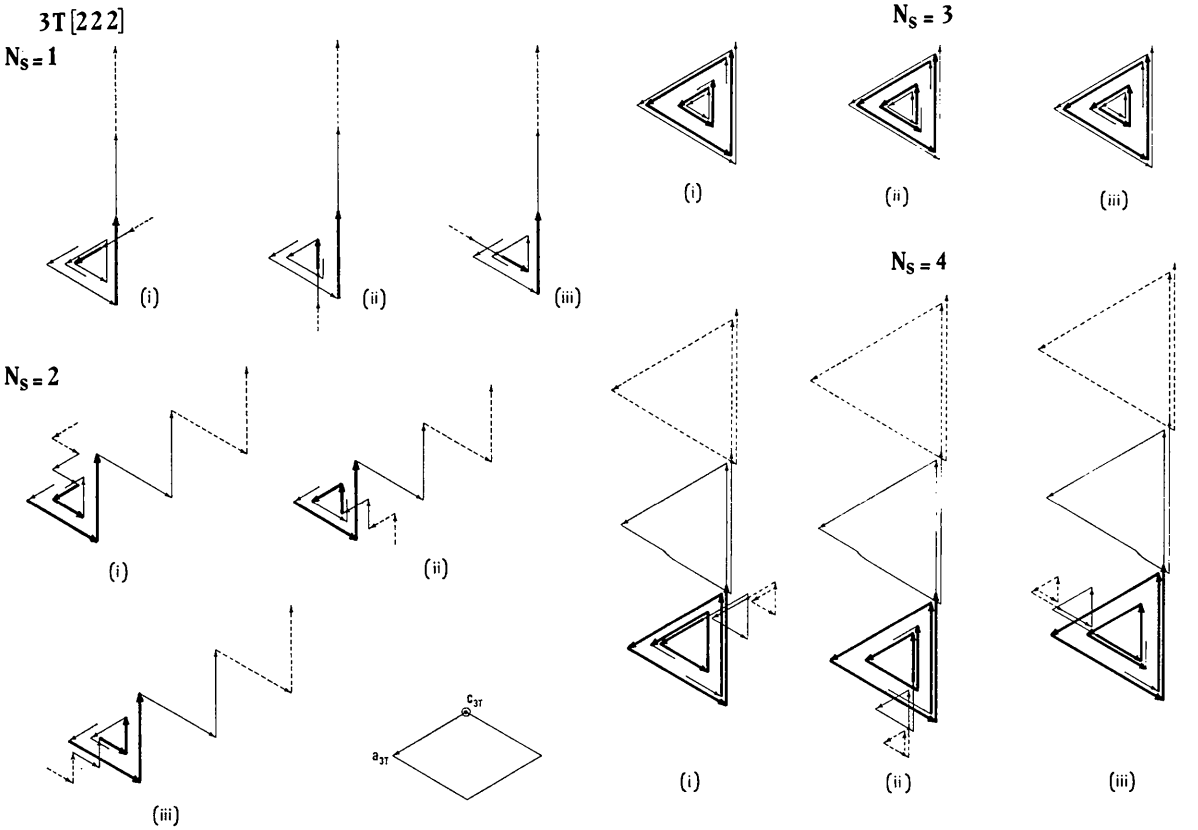

Fig. 5. Spirals on $3T[222]$, $N_s = 1$ to 5. A perspective representation is adopted here: $\mathbf{t}_n$ modulus becomes larger from bottom to top. For full explanation of symbols, see caption to Fig. 3.

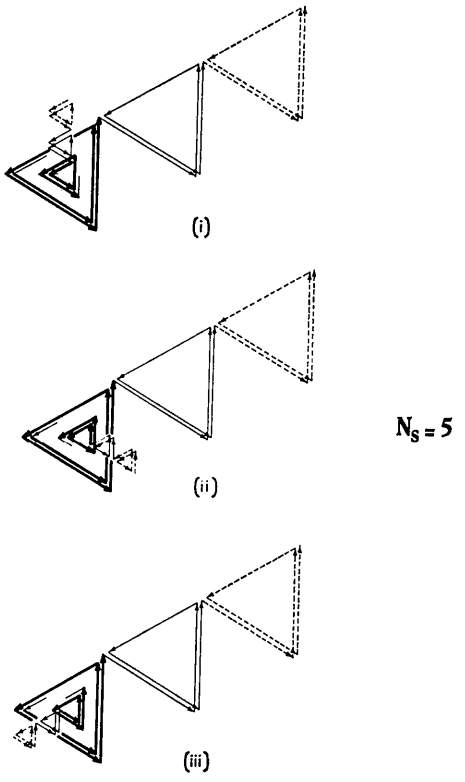

Fig. 5 (*cont.*)

II.4 *Complex polytypes and spiral growth*

About 20 complex polytype stacking sequences have been reported so far in the literature (Table 7). The scope of this section is to compare these sequences with those predicted by the present extension of the dislocation theory of polytypism on micas. Up to now, the more extended studies of layer-stacking sequences have been carried out using X-ray single-crystal methods (Ross *et al.*, 1966; Takeda, 1967*b*). All possible 'unmodulated periodic intensity distributions' that are characteristic of stacking sequences are calculated and compared with intensity distributions observed along certain of the reciprocal-lattice rows parallel to **c***. Nevertheless, the latter powerful method gives little information on the growth-mechanism–polytypism relationships as long as it is not completed by surface and/or volume characterization of the studied sample. Recently (Baronnet, 1972; Baronnet *et al.*, 1975), it was possible to analyse some polytype stacking sequences of synthetic micas using spiral step configurations on an {001} form of these crystals. Spiral growth appears to be a very common growth mechanism of synthetic micas grown under hydrothermal conditions. Therefore there is a great temptation to account for the origin of the complex polytypes listed in Table 7 in the light of the dislocation theory of polytypism. Ascertaining that complex mica polytypes are frequently based on $1M[0]$, $3T[222]$ and probably $2M_1[2\bar{2}]$, Takeda (1971) suggested that this latter theory is operative among micas.

Table 7. *A review of complex mica polytypes*

Complex polytype	Space group*	Structural series	Species	References
$3Tc[02\bar{2}]$	$C\bar{1}$		Siderophyllite	Ross *et al.* (1966)
$4Tc[(0)_2 2\bar{2}]$	$C\bar{1}$			Takeda (1969)
$8Tc[(0)_6 2\bar{2}]$	$C\bar{1}$	$n+2Tc[(0)_n 2\bar{2}]$	Oxybiotite	Ross *et al.* (1966)
$9Tc[(0)_7 2\bar{2}]$	$C\bar{1}$		Li–Fe mica	Rieder (1970)
$14Tc[(0)_{12} 2\bar{2}]$	$C\bar{1}$		Oxybiotite	Ross *et al.* (1966)
$23Tc[(0)_{21} 2\bar{2}]$	$C\bar{1}$		Oxybiotite	Ross *et al.* (1966)
$3Tc[02\bar{2}]$	$C\bar{1}$	$2n+1Tc[0(2\bar{2})_n]$	Synth. OH-muscovite	Baronnet *et al.* (1975)
$3Tc[0\bar{2}2]$	$C\bar{1}$	$2n+1Tc[0(\bar{2}2]_n)$	Synth. OH-muscovite	Baronnet *et al.* (1975)
$5Tc[0(\bar{2}2)_2]$	$C\bar{1}$		Synth. OH-muscovite	Baronnet *et al.* (1975)
$8Tc[(2\bar{2})_3\bar{2}2]$	$C\bar{1}$	$2n+2Tc[(2\bar{2})_n\bar{2}2]$	Biotite	Hendricks & Jefferson (1939), Smith & Yoder (1956), Takeda (1969)
$4M[2220]$	$C2$	$3n+1M[(222)_n 0]$	Oxybiotite	Ross *et al.* (1966)
$5M[(222)2\bar{2}]$	$C2$		Li–Fe mica	Rieder (1970)
$8M[(222)_2 2\bar{2}]$	$C2$	$3n+2M[(222)_n 2\bar{2}]$	Oxybiotite	Ross *et al.* (1966)
$11M[(222)_3 2\bar{2}]$	$C2$		Oxybiotite	Ross *et al.* (1966)
$14M[(222)_4 2\bar{2}]$	$C2$		Li–Fe mica	Rieder (1970)
$8Tc[(0)_3 2\bar{2}\bar{2}02]$	$C1$		Oxybiotite	Ross *et al.* (1966)
or $[(0)_3 20\bar{2}22]$	$C1$		Oxybiotite	Takeda (1969)
$10Tc[(2)_5\bar{2}2200]$	$C1$		Oxybiotite	Ross *et al.* (1966)
or $[(2)_5 00222]$	$C1$		Oxybiotite	Takeda (1969)
$4Tc[0132]$	$C1$		Synth. Li-fluorophlogopite	Takeda (1967 *a*, *b*) Takeda & Donnay (1965)
$18Tc[(0)_{n_1-1}2(0)_{n_2-1}\cdots 2(0)_{n_3-1}2]$ with $n_3<n_1<n_2$ $n_1+n_2+n_3=18$			Biotite	Dekeyser & Amelinckx (1955)

* Space groups are derived according to criteria developed by Takeda (1971), p. 1048.

Thus, structural terms of the series $n+2$ $Tc[(0)_n2\bar{2}]$ may originate from a $N_s=n+2$-layered spiral operating on a single-layer faulted $1M[0]$ basic structure (structure of the exposed ledge). Note that this single layer, in fault position with the two adjoining layers above and below it, forms a local $2M_1[2\bar{2}]$ sequence in syntaxic coalescence with $1M[0]$, a not surprising configuration for oxybiotite and lithium–iron micas.

The two enantiomorphic series $2n+1$ $Tc[0(2\bar{2})_n]$ and $2n+1$ $Tc[0(\bar{2}2)_n]$ are respectively the same as the series $N_sTc[(2\bar{2})_{(N_s-1)/2}0]$ and $N_sTc[(\bar{2}2)_{(N_s-1)/2}0]$ theoretically deduced from $N_s=2n+1$ layered dislocations operating on a perfect $2M_1[2\bar{2}]$ structure. The $2n+2$ $Tc[(2\bar{2})_n\bar{2}2]$ polytype may be derived from a spiral whose pitch is $N_s=2n+2$, operating on a single-layer faulted $2M_1[2\bar{2}]$ basic structure. This single layer with the help of its first and second underlying layers induces a local $3T[222]$ arrangement in syntaxic coalescence with $2M_1[2\bar{2}]$. The two $3n+1$ $M[(222)_n0]$ and $3n+2$ $M[(222)_n2\bar{2}]$ series were reported as $N_sM[(222)_{(N_s-1)/3}0]$ and $N_sM[(222)_{(N_s-2)/3}2\bar{2}]$ respectively in the present theoretical analysis concerning polytype structures generated from the perfect $3T[222]$ basic structure. Six layers stacked according to the $3T[222]$ scheme completed by four layers in the $1Mr$ $n(120)$ configuration may be involved in the exposed ledge of a 10-layered screw dislocation in order to explain the occurrence of the $10Tc[(2)_5\bar{2}2200]$ or $[(2)_500022\bar{2}]$ polytype. $8Tc[(0)_32\bar{2}\bar{2}02]$ or $[(0)_320\bar{2}\bar{2}2]$ may be more easily explained by an eight-layered spiral arising on a $1Mr$ $n(120)$ or heavily faulted $1M[0]$ parent structure. In spite of its low periodicity, the stacking sequence of the $4Tc[0231]$ polytype suggests the activity of a four-layered spiral on the $1Mr$ $n(60)$ aperiodic structure. Finally, the doubtful $18Tc[(0)_{n_1-1}2(0)_{n_2-1}2(0)_{n_3-1}2]$ would be produced by a 18-layered spiral ledge exposing a twice-twinned $1M[0]$ basic structure: composition plane (001), twin axis $[3\bar{1}0]$. Note that the winding up of this last stacking sequence results in a polysynthetic twinning of the $1M[0]$ structure. Following Sadanaga & Takeuchi (1961), this twinning mode may be denominated as 'spiral twin'.

The complex polytypes reported above have been interpreted in the light of a single screw dislocation arising on the crystal but some of them could have been explained using cooperation spiral groups (Dekeyser & Amelinckx, 1955; Baronnet, 1972*b*).

III. Discussion

The theoretical derivation of polytypes issued from various strength dislocations in the different assumed basic structures of micas shows that:

(1) further growth of a periodic basic structure occurs commonly* owing to its low periodicity;

(2) new polytypes based on the basic structure may be created. Among them, long-period polytypes (L.P.P.) for high N_s values and short-period polytypes (S.P.P.) for low N_s values may be distinguished. S.P.P. are of particular interest here. The same S.P.P. stacking sequence may be obtained when dislocations of very feeble strength are active on different basic structures. For instance, $1M[0]$ is generated by $N_s=1$ on $1M[0]$, $2M_1[2\bar{2}]$, $2M_2[1\bar{1}]$, $2O[33]$, $3T[222]$, $3T[\bar{2}\bar{2}2]$, $1Mr$ $n(120)$ and $1Mr$ $n(60)$ whereas $2M_1[2\bar{2}]$ appears from $N_s=2$ on $2M_1[2\bar{2}]$, $3T[222]$, $3T[\bar{2}\bar{2}2]$ and eventually $1Mr$ $n(120)$ and $1Mr$ $n(60)$. Spiral growth patterns of $1M[0]$, $2M_1[2\bar{2}]$ and $3T[222]$ S.P.P. were reported by Baronnet (1972*b*) on synthetic OH-phlogopite crystals of $1Mr$ $n(120)$ basic structure. It may be noted that S.P.P. admit the same stacking sequences as mica polymorphs or basic structures, but must be distinguished from each other from the growth point of view. Basic structures or polymorphs in the structural sense are built up during the nucleation and/or layer-growth stages (Baronnet, 1972*a*, *b*; Baronnet *et al.*, 1975) whereas S.P.P. and L.P.P. originate during the subsequent spiral growth process. Güven (1971) emphasizes the interrelationships that may exist between the actual structure of the single layer and its regular stacking sequence in dioctahedral micas. If this statement holds for basic structures or polymorphs, to what extend it may be valid for S.P.P. is not clear. However in this latter case, the actual single-layer structure is more or less inherited from the previous basic structure so that, for instance, the $2M_1[2\bar{2}]$ S.P.P. may possibly have a different single-layer structure depending upon whether it is derived from $N_s=2$ on $2M_1[2\bar{2}]$ or on $3T[222]$.

In the above derivation of polytypes, we have considered the structure of the dislocated crystal as a whole. Accordingly, it was shown that, in the more general case, the sample consists of three structural parts, *i.e.* the basic structure sandwiched by two spiral-grown structures. This behaviour may possibly explain part of such structural features as 'epitaxic overgrowths' (Rieder, 1970; Ramdohr & Strunz, 1967) and macroscopic twinning commonly reported in mica literature. Different polytypes or polymorphs coalescing in the same crystal and not symmetry-related are reported as epitaxic overgrowths. Some examples were described by Rieder (1970) in natural Fe–Li micas. Figs. 4 and 5 of the present paper show obviously that the coalescence of two structures in the following mutual orientations reported below may be due to spiral growth: $1M$–$2M_1$ with $[100]_{1M}\|[\bar{1}\bar{1}0]_{2M_1}$ or $[\bar{1}10]_{2M_1}$; $1M$–$2M_2$ with $[100]_{1M}\|[\bar{1}\bar{1}0]_{2M_2}$ or $[\bar{1}10]_{2M2}$; $1M$–$2O$ with $[100]_{1M}\|[100]_{2O}$ or $[\bar{1}00]_{2O}$; $1M$–$3T$ with $[100]_{1M}\|\langle 10\bar{1}0\rangle_{3T}$ and $2M_1$–$3T$ with $[100]_{2M_1}\|\langle 10\bar{1}0\rangle_{3T}$.

A particular growth process of mica twins may be considered on the basis of the above theoretical derivations: let us suppose that a screw dislocation of Burgers-vector strength $N_s=1$ appears on the basic $2M_1[2\bar{2}]$ structure at the moment when the latter is only built of two single layers ($N_c=2$). The two associated spirals on both {001} faces will induce two

* A detailed discussion of spiral-grown polytype frequencies will be published in the forthcoming part II of this paper.

twinned $1M$[0] individuals: helicoidal composition plane (001), twin axis [3$\bar{1}$0] or [310]. The same process ($N_c=3$, $N_s=2$) on the basic $3T$[222] structure will lead to two $2M_1$[2$\bar{2}$] individuals twinned according to the same twin law. In the same manner, $N_c=2$, $N_s=1$ on $2M_2$[1$\bar{1}$] and $2O$[33] will result in two $1M$[0] individuals respectively twinned (001), [1$\bar{1}$0] or [110] and (001), [100].

The interpretation of complex mica polytypes reported so far in the literature (Table 7), in the light of the single-dislocation theory of polytypism reveals that the structure of the exposed ledge may be a part of either a perfect or more or less faulted basic structure or may require the coalescence of two different ones. These results are consistent with more or less complete structural control (Smith & Yoder, 1956) over the nature and perfection of the basic structure depending upon the composition and/or growth parameters of the mica concerned during the layer-growth stage. We note that this structural control may change during the growth of a single sample. Recently, it was shown in SiC (Krishna & Marshall, 1971), CdI_2 (Lal & Trigunayat, 1971; Tiwari & Srivastava, 1972) and ZnS (Mardix, Kalman & Steinberger, 1968) that polytypic transformations in the solid state are possible. These transformations occur through the introduction of ordered stacking faults into the parent structure. This mechanism implies the nucleation and expansion of planar faults bounded by partial dislocations. In the trioctahedral mica case, Takeuchi & Haga (1971) worked out a theory of geometrical interest based upon periodic slips localized in the octahedral sheet of the mica structure. The physical significance of this slip mechanism seems rather hazardous since glide occurs much more easily in the interlayer region as shown by detailed studies of perfect (Cartz & Tooper, 1965; Silk & Barnes, 1961; Willaime & Authier, 1966) and partial (Caslavsky, 1969) dislocations in micas by electron microscopy and X-ray topography. Furthermore, attempts to transform biotite polytypes by annealing (Takeuchi & Haga, 1971) remain unsuccessful. All the above mentioned considerations lead us to consider mica complex polytypism as uniquely a growth phenomenon.

Critical comments from Drs H. Takeda, Tokyo University, M. Ross, U.S. Geological Survey, and N. Güven, Texas Tech. University, have resulted in improvements of the manuscript. Thanks are also due to Drs W. L. Brown, University of Nancy I, and B. Velde, University of Paris VI, for their interest in this paper content as well as for their improvements of the English language.

References

AMELINCKX, S. & DEKEYSER, W. (1953). *C.R. XIXème Congr. Geol. Int.* pp. 9–22 (*Mineral. Abs.* **12**, 520).
BARONNET, A. (1972*a*). *C.R. Acad. Sci. Paris.* **274**, 785–787.
BARONNET, A. (1972*b*). *Amer. Min.* **57**, 1272–1293.
BARONNET, A. (1973). *J. Cryst. Growth*, **19**, 193–198.
BARONNET, A., AMOURIC, M. & CHABOT, B. (1975). In preparation.
CARTZ, L. & TOOPER, B. (1965). *J. Appl. Phys.* **36**, 2783–2787.
CASLAVSKY, J. L. (1969). Ph. D. Thesis, Pennsylvania State Univ.
DEKEYSER, W. & AMELINCKX, S. (1955). *Les Dislocations et la Croissance des Cristaux.* Paris: Masson.
FOSTER, M. D. (1960). *U.S. Geol. Surv. Prof. Pap.* **354-E**, 115–147.
FRANK, F. C. (1949). *Discuss. Faraday Soc.* **5**, 48–54, 66–68.
FRANK, F. C. (1951). *Phil. Mag.* **42**, 1014–1021.
GIUSEPPETTI, G. & TADINI, C. (1972). *Mineral. petrogr. Mitt.* **18**, 169–184.
GÜVEN, N. (1971). *Clays Clay. Min.* **19**, 159–165.
HENDRICKS, S. B. & JEFFERSON, M. E. (1939). *Amer. Min.* **24**, 729–771.
JACKSON, W. W. & WEST, J. (1931). *Z. Kristallogr.* **76**, 211–227.
JACKSON, W. W. & WEST, J. (1933). *Z. Kristallogr.* **85**, 160–164.
KRISHNA, P. & MARSHALL, R. C. (1971). *J. Cryst. Growth*, **11**, 177–181.
KRISHNA, P. & VERMA, A. R. (1965). *Z. Kristallogr.* **121**, 36–54.
LAL, G. & TRIGUNAYAT, G. C. (1971). *J. Cryst. Growth.* **11**, 177–181.
MARDIX, S., KALMAN, Z. H. & STEINBERGER, I. T. (1968). *Acta Cryst.* A**24**, 464–469.
MITCHELL, R. S. (1957). *Z. Kristallogr.* **109**, 1–28.
MUNOZ, J. L. (1968). *Amer. Min.* **53**, 1490–1512.
PABST, A. (1955). *Amer. Min.* **40**, 967–974.
PAULING, L. (1930). *Proc. Natl. Acad. Sci. U.S.* **16**, 123–129.
RAMDOHR, P. & STRUNZ, H. (1967). *Klogksmanns Lehrbuch der Mineralogie*, p. 189. Stuttgart: Ferdinand Enke Verlag.
RAMSDELL, L. S. (1947). *Amer. Min.* **32**, 64–82.
RIEDER, M. (1970). *Z. Kristallogr.* **132**, 161–184.
ROSS, M., TAKEDA, H. & WONES, D. R. (1966). *Science*, **151**, 191–193.
SADANAGA, R. & TAKEUCHI, Y. (1961). *Z. Kristallogr.* **116**, 406–429.
SILK, E. C. H. & BARNES, R. S. (1961). *Acta. Met.* **9**, 558–562.
SMITH, J. V. & YODER, H. S. (1956). *Miner. Mag.* **31**, 209–235.
TAKEDA, H. (1967*a*). *J. Miner. Soc. Japan*, **8**, *Spec. Issue* n° 1 pp. 39–41.
TAKEDA, H. (1967*b*). *Acta Cryst.* **22**, 845–853.
TAKEDA, H. (1969). Autumn Meeting Mineral. Soc. Japan (abstract).
TAKEDA, H. (1971). *Amer. Min.* **56**, 1042–1056.
TAKEDA, H. & DONNAY, J. D. H. (1965). A. C. A. Program and Abstracts, Winter Meeting, Suffern, N.Y. 23.
TAKEDA, H. & MACKAY, A. L. (1969). *J. Miner. Soc. Japan*, **9**, 357.
TAKEUCHI, Y. & HAGA, N. (1971). *J. Miner. Soc. Japan, Spec. Pap.* **1**, 74–87.
TIWARI, R. S. & SRIVASTAVA, O. N. (1972). *J. Appl. Cryst.* **5**, 347–352.
VERMA, A. R. & KRISHNA, P. (1966). In *Polymorphism and Polytypism in Crystals.* New York: John Wiley.
WILLAIME, C. & AUTHIER, A. (1966). *Bull. Soc. fr. Minér. Crist.* **89**, 269–270.
ZVYAGIN, B. B. (1962). *Sov. Phys. Crystallogr.* **6**, 571–580.